

Statistical Analysis of 5G Channel Propagation using MIMO and Massive MIMO Technologies

Zaid Ahmed Shamsan

Electrical Engineering Department

College of Engineering

Imam Mohammad Ibn Saud Islamic University (IMSIU)

Riyadh, Saudi Arabia

shamsan@ieee.org

Abstract—Multiple Input Multiple Output (MIMO) and massive MIMO technologies play a significant role in mitigating five generation (5G) channel propagation impairments. These impairments increase as frequency increases, and they become worse at millimeter-waves (mmWaves). They include difficulties of material penetration, Line-of-Sight (LoS) inflexibility, small cell coverage, weather circumstances, etc. This paper simulates the 5G channel at the E-band frequency using the Monte Carlo approach-based NYUSIM tool. The urban microcell (UMi) is the communication environment of this simulation. Both MIMO and massive MIMO use uniformly spaced rectangular antenna arrays (URA). This study investigates the effects of MIMO and massive MIMO on LoS and Non-LoS (NLoS) environments. The simulations considered directional and omnidirectional antennas, the Power Delay Profile (PDP), Root Mean Square (RMS) delay spread, and small-scale PDP for both LoS and NLoS environments. As expected, the wide variety of the results showed that the massive MIMO antenna outperforms the MIMO antenna, especially in terms of the signal power received at the end-user and for longer path lengths.

Keywords—MIMO; massive MIMO; millimeter-waves; channel propagation; path loss exponent; RMS delay spread; received power

I. INTRODUCTION

Massive Multiple Input Multiple Output (MIMO) and Millimeter-waves (mmWaves) are two key technologies of 5G wireless systems that deliver high data rates, support multiple users, and provide very low latency. The use of mmWaves for the 5G systems is still in the experimental stage. Classically, the mmWaves belong to the frequency spectrum from 30 to 300GHz [1]. Some frequency bands of the first part of this frequency spectrum, up to 100GHz (as well as the traditional wireless mobile generation bands) are dedicated to the 5G system because they offer a huge amount of unutilized or under-utilized spectrum frequencies, compared to the lower bands. The E-band (71-76 and 81-86GHz) [2, 3] can be represented by 73GHz and it is one of the main frequencies allocated to 5G systems. It is well recognized that the spectral bandwidth is directly proportional to the amount of transmitted data rate. However, using the mmWaves for mobile communication exposes several propagation challenges, e.g.

signal attenuation, coverage area limitations, and, most notably, high penetration losses. Due to the higher frequency of mmWaves, free space loss is much higher especially when an isotropic antenna is used, and many materials cause very high absorption loss, while diffraction is less noticeable. Consequently, mmWave signal goes under high blockage, and most of the time propagation tends to be Line-of-Sight (LoS) - based [4]. To mitigate mmWave disadvantages, several technologies have been introduced, such as small cell coverage, beamforming, MIMO and massive MIMO antennas, etc. Massive MIMO-OFDM has been considered as one of the most desired technologies for broadband wireless systems and is worldwide recognized as the 5G wireless communication basis. It is more flexible and adaptable to stay active, especially if developed for a high number of antennas or massive MIMO [1, 3].

This paper will discuss the 73GHz channel and signal propagation using MIMO and massive MIMO technologies in urban microcell area. In [5], the 73GHz frequency band proved to be power-efficient and robust against atmospheric variations. Both omnidirectional and directional channel models were used due to the fact that they are widely adopted by the industry and researchers for proper designing of wireless systems and antenna arrays in supporting massive MIMO systems by employing spatial diversity and/or beamforming gain respectively [6, 7]. For this purpose, the Monte Carlo approach-based NYUSIM simulator (NYUSIM v3.0) was utilized to apply MIMO-Orthogonal Frequency-Division Multiplexing (OFDM) and massive MIMO technologies and generate Channel Impulse Responses (CIRs) from both omnidirectional and directional channel models at 73GHz [8-10]. This simulator can be also used in the THz band [11].

II. MIMO AND MASSIVE MIMO TECHNOLOGIES

Generally, three methods can be planned to improve the wireless network efficiency, namely deploying extreme access points, using wide frequency spectrum, and increasing the spectral efficiency. The foreseen wireless systems will utilize small base station coverage and thus will require by default many access points to cover all considered areas. Also, new spectral bands will be exploited to support the efficiency of the wireless network. However, the spectral efficiency always

Corresponding author: Zaid A Shamsan

needs to be maximized in a given frequency band. The spectral efficiency equals to the total bits that can be sent per second in each unit of bandwidth (bits/s/Hz) which ultimately contributes in improving the throughput (Th) [12]:

$$Th = BW \times S_e \quad (1)$$

where BW is the bandwidth (Hz) and S_e is the spectral efficiency (bits/s/Hz). A recognized technique to raise the spectral efficiency is to exploit the concept of multiple antennas at the transceivers. Communication with multiple antennas leads to send out multiple streams which in turn cause multiplexing gain that significantly improves the capacity of communication. Therefore, the use of MIMO antennas as a diversity method is able to improve the communication reliability. The useful characteristics of the MIMO technology allowed its incorporation to the new generation wireless systems (4G, 5G, and 6G). Figure 1 shows the MIMO technology concept for point to point link.

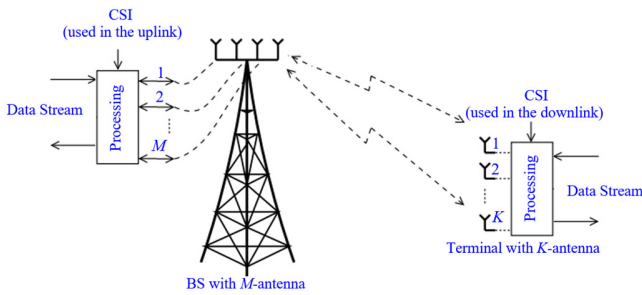


Fig. 1. MIMO technology for point to point link (up- and down-link).

In each channel of the MIMO technology, one vector is transmitted and another is received. If an additive white Gaussian noise (AWGN) at the receiver (Rx) exists, Shannon theory gives the following equations for the spectral efficiency of the link (in b/s/Hz):

$$C^{ul} = \log_2 \left| \mathbf{I}_M \frac{\rho_{ul}}{K} \mathbf{G} \mathbf{G}^H \right| \quad (2)$$

$$C^{dl} = \log_2 \left| \mathbf{I}_K \frac{\rho_{dl}}{M} \mathbf{G}^H \mathbf{G} \right| \\ = \log_2 \left| \mathbf{I}_M \frac{\rho_{dl}}{M} \mathbf{G} \mathbf{G}^H \right| \quad (3)$$

where M is the number of BS antennas, K is the number of terminal antennas, \mathbf{G} is an $M \times K$ matrix for the channel frequency response between the Base Station (BS) array and the terminal array, and ρ_{ul} and ρ_{dl} are the signal-to-noise ratios (SNRs) for the uplink and downlink, which are proportional to the corresponding total radiated powers. The spectral efficiency values in (2) and (3) involve that the Rx must know \mathbf{G} , however the transmitter (Tx) does not require knowing \mathbf{G} . If the Tx attains Channel State Information (CSI), the performance will be enhanced. The spatial multiplexing gain has been exploited and the MIMO was developed to the multiuser MIMO (MU-MIMO), where the number of users is concurrently functioned by one BS supported by multiple MIMO antennas [13-16]. By equipping the BS with more antennas, more degrees of freedom can be provided and therefore, more users can concurrently connect in the same resource of time-frequency.

Consequently, a large sum throughput can be attained. When a BS is enhanced with 100 or more antennas concurrently (MU-MIMO system) to serve tens (or more) of users in the same time-frequency resource, this system is termed as a Massive MIMO, very large MU-MIMO, hyper-MIMO, or full-dimension MIMO [12]. Precisely, in contrast, MU-MIMO systems support a large number of wireless broadband terminals using a large number of BS antennas whereas, massive MIMO is a type of MU-MIMO system where antennas (hundreds/thousands) concurrently serve wireless broadband terminals (tens/hundreds) in the same frequency resource as shown in Figure 2. Assuming that terminals in MU MIMO/Massive MIMO have a single antenna as shown in Figure 2 in which the BS serves K terminals, let \mathbf{G} be a matrix of $M \times K$ matching the frequency response between the BS array and the K terminals. The sum spectral efficiencies of the up- and down-link are expressed by:

$$C^{ul} = \log_2 |\mathbf{I}_M + \rho_{ul} \mathbf{G} \mathbf{G}^H| \quad (4)$$

$$C^{dl} = \max_{\substack{v_k \geq 0 \\ \sum_{k=1}^K v_k \leq 1}} \log_2 |\mathbf{I}_M + \rho_{dl} \mathbf{G} \mathbf{D}_v \mathbf{G}^H| \quad (5)$$

where $\mathbf{v} = [v_1, \dots, v_K]^T$, ρ_{ul} is the uplink SNR per each terminal, and ρ_{dl} is the downlink SNR. The calculation of downlink capacity needs a solution of the convex optimization problem. The attaining of CSI is essential to (4) and (5). The BS must identify the channels in the uplink, and each terminal has to be informed its allowed transmission rate individually, while in the downlink, the BS and the terminals must have CSI [17].

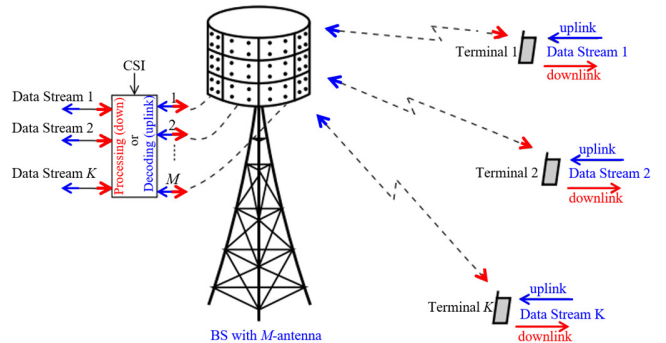


Fig. 2. Massive MIMO system (up- and down-link).

III. MODELS OF CHANNEL PROPAGATION

The NYUSIM simulator uses two main integrated models: the free space Path Loss (PL) model and the Statistical Spatial Channel Model (SSCM). The Close-In (CI) free space PL model used in this paper as shown in (6) is based on Friis' and Bullington's research work that set wireless propagation fundamental principles, where the path loss depends on the environment with a reference distance and includes an additional attenuation component [18-19]:

$$PL^{CI}(f, d_{3D}) = 32.4 + 20 \log_{10}(f) + 10n \log_{10}(d_{3D}) + L_s + \chi_{\sigma}^{CI} \quad (6)$$

where f is the operation frequency (GHz), n denotes the Path Loss Exponent (PLE), d_{3D} is the three-dimension (3D) distance

between the Tx and Rx, and d_0 is the free space reference distance, ranging between 1m and 5m (1m in this paper), provided that $d_{3D} \geq d_0$. The term χ_{σ}^{cl} represents the Gaussian random variable with zero-mean and standard deviation σ in dB, while L_s denotes the atmospheric conditions attenuation factor [1, 8], and d_{3D} is defined as in (6). The adopted model of the channel (closed-in path loss) uses a small number of parameters compared to that of 3GPP/ITU channel models while it can estimate a wide range of microwave and mmWave frequencies, physical separation paths, and scenarios with better performance, better stability, and fewer parameters. The PLE is confidentially relevant to the environment where the communication system works. It has different values for different PL models which are developed through numerical schemes combined with empirical approximations of experimental data obtained in channel sounding measurements. For instance, for the urban microcell (UMi) scenario and in the case of LoS free space environment, the PLE is set to be 2 with a shadow fading standard deviation of 4.0dB, whereas these two parameters are respectively set to 3.2 and 7.0dB in the NLoS environment. In the SSCM model, time clusters and spatial lobes are employed to model the omnidirectional CIR, and power spectra of both Angle of Departure (AoD) and Angle of Arrival (AoA). Time clusters contain multipath components moving closely in time, and the ones which arrive from different angular directions in a short excess delay time. Spatial lobes are the main directions of arrival or departure components that arrive or depart within several hundreds of nanoseconds. In the SSCM model, multiple paths within a time cluster can arrive at unique pointing angles that can be detected by directional antennas with high gain [1, 18]. In fact, the number of clusters of the mmWave signals should not be large due to the fact that this can cause an imprecise spectral efficiency prediction. Thus, the number of time clusters is in the range 1–6, whereas the spatial lobes are between 2 and 5 [18].

IV. COMMUNICATION SCENARIOS WITH MIMO AND MASSIVE MIMO

Several studies on MIMO and massive MIMO have been conducted in order to develop and improve the technology of communication [1, 20-22]. The proposed communication scenario is a communication link in an urban microcell system at 73GHz using 4×4 MIMO and 64×64 massive MIMO technologies. It is assumed that both the Tx and Rx are equipped with 4 MIMO or 64 massive MIMO antenna elements comprising uniformly spaced rectangular antenna arrays (URA) with M_x and M_y antenna elements in the elevation domain and azimuth domain, in that order [23]. The adopted antenna patterns are based on Table 7.3-1 of [24]. For OFDM technique, each subcarrier has a MIMO channel coefficient which will be generated through paramount parameters of each solvable multipath component. The MIMO channel coefficients $h_{p,m,l}(f)$ between the M_y Tx antenna and the k^{th} Rx antenna for the subcarrier f are expressed through the following equation [1, 8]:

$$h_{p,m,l}(f) = \sum_p \alpha_{m,k,p} e^{j\Phi_{m,k,p}} \times e^{-j2\pi f \tau_{m,k,p}} \times e^{-j2\pi d_T m \sin(\phi_{m,k,p})} \times e^{-j2\pi d_R k \sin(\varphi_{m,k,p})} \quad (7)$$

where p represents the p^{th} resolvable solvable multipath component, α represents the amplitude of the channel gain, Φ is the phase of the multipath component, τ is the time delay, d_T and d_R denote the antenna element spacing at the Tx and Rx respectively, whereas ϕ and φ represent the azimuth AoD and AoA correspondingly. It is assumed that the number of carriers is 1601 (the frequency interval between adjacent subcarriers is 500kHz and the bandwidth is 800MHz, therefore, $(800\text{MHz}/500\text{kHz}) + 1 = 1601$ subcarriers).

V. THE MAIN PARAMETERS

In Table I, the Tx and Rx antenna types, simulation conditions, propagation parameters, and system components are tabulated. The results of applying the assumed values in Table I will be discussed in the next section.

TABLE I. KEY PARAMETERS AND SIMULATION CONDITIONS [1, 8, 9, 18, 25, 26]

Parameter	Value	Parameter	Value
Operation frequency (GHz)	73	Tx and Rx antenna gain (dBi)	24.9
No. of Tx and Rx antenna elements in Massive MIMO	64×64	No. of Massive MIMO antenna elements per row	8
System bandwidth (MHz)	800	Tx and Rx array type	URA
No. of Tx and Rx antenna elements in MIMO	4×4	Tx and Rx antenna elevation HPBW	8.6°
Tx and Rx antenna azimuth HPBW	10.9°	No. of MIMO antenna elements per row	2
Tx power (dBm)	30	Tx and Rx antenna spacing	0.5λ
Barometric pressure (mbar)	1013.25	OFDM subcarrier spacing (kHz)	500
Humidity	50%	No. of OFDM subcarriers	1601
Temperature	20°C	Polarization	Co-Pol

VI. RESULTS AND DISCUSSION

Figures 3(a)-(d) explain the substantial difference in the omnidirectional and directional path loss at different environments and number of antenna elements at 300m separation distance between the Tx and Rx and operation frequency of 73GHz. These figures are produced using the NYUSIM tool, where the PL, PLE(n), and directional shadow fading standard deviation are demonstrated for 4 LoS and NLoS cases. Each Figure illustrates the PL, n , and directional standard deviation. It can be seen that the Tx antenna gain and Rx antenna gain for the urban microcell are assumed to be the same (24.9dBi). From Figure 3(a), it can be noticed that the omnidirectional path loss at 300m is roughly 123.5dB using MIMO in LoS environment, while it increases to 164.4dB with MIMO in NLoS environment at the same distance (Figure 3(b)). This means that there is a very large difference of 40.9dB in the PL in the case of LoS compared to NLoS. On the other hand, the omnidirectional PL massive MIMO is approximately 116.6dB in LoS environment, while it increases to 153.3dB in NLoS environment at the same distance as displayed in Figures 3(c) and 3(d) respectively. The difference between the two environments is approximately 36.7dB. Table II shows a comparison among the 4 cases of the systems used in the simulations. It can be stated that the PL in the case of MIMO in NLoS is the largest, while the lowest PL occurs using massive MIMO in LoS environment. Table II shows the difference in omnidirectional PL among the system scenarios.

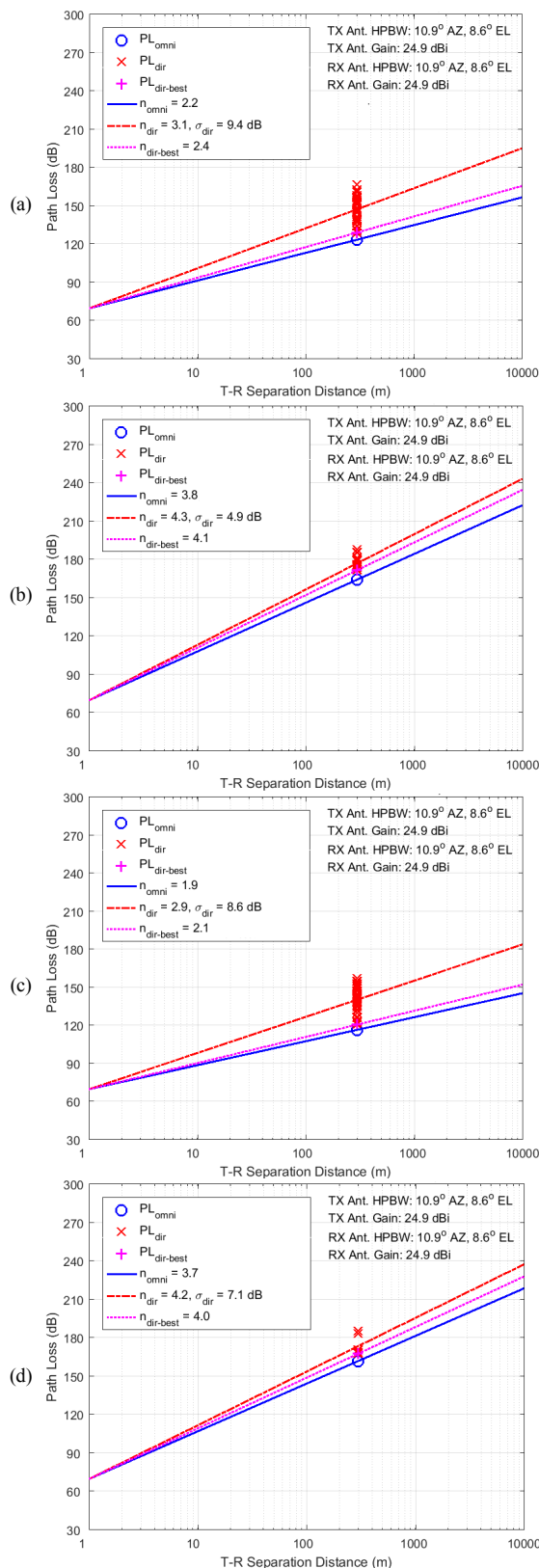


Fig. 3. Omnidirectional and directional path loss Tx-Rx separation distance for an urban microcell scenario (a) 4x4 MIMO LoS, (b) 4x4 MIMO NLoS, (c) 64x64 Massive MIMO LoS, (d) 64x64 Massive MIMO NLoS.

TABLE II. DIFFERENCE IN OMNIDIRECTIONAL PL AMONG THE SYSTEM SCENARIOS

Description	Difference in omnidirectional PL (dB)			
	MIMO-LoS	MIMO-NLoS	Massive MIMO-LoS	Massive MIMO-NLoS
MIMO-LoS	----	-40.9	6.9	-29.8
MIMO-NLoS	40.9	----	47.8	11.1
Massive MIMO-LoS	-6.9	-47.8	----	-36.7
Massive MIMO-NLoS	29.8	-11.1	36.7	----

To study the effect of the directional antenna compared to the omnidirectional antenna, the worst case of MIMO system is considered to investigate its impact on the RMS delay spread. This scenario is shown in Figure 4 for the LoS environment in which the maximum separation distance between the Tx and the Rx is 0.5km. The directional antenna clearly seems that it causes less RMS delay spread. Figure 4 shows that the maximum RMS delay spread is 2.8ns when the Rx is located at 400m whereas the minimum RMS delay spread is about 0.3ns at a separation distance of 250m and 450m from the Tx. In contrast, the omnidirectional antenna causes greater RMS delay spread for all cases. The maximum RMS delay spread for the omnidirectional antenna is 24ns at 100m whereas the minimum value of the antenna, 9.5ns, is at 500m. These results reveal that the RMS delay spread resultant from omnidirectional antenna is always greater than that of the directional antenna. Moreover, Figure 4 indicates that there is very small fluctuation in the delay generated by the directional antenna, however, the omnidirectional antenna generates a high RMS delay fluctuation. The same scenario is shown in Figure 5 for the MIMO system to investigate the impact of the NLoS environment on the RMS delay spread. The RMS delay spread values in Figure 5 are higher than that in Figure 4. In addition, the fluctuations of RMS delay spread values in the NLoS environment are higher than that in the LoS environment which creates more stable delay. Furthermore, this result is similar for either omnidirectional or directional antenna type, the general effect of NLoS does not change. For example, the directional RMS delay shown in Figure 6 for NLoS is almost higher than that of LoS except very few cases where the RMS delay is higher than that of NLoS by a very small value of RMS delay spread. This is true due to the fact that the nature of NLoS environment is filled with several reflectors, scatters, diffracted materials, etc.

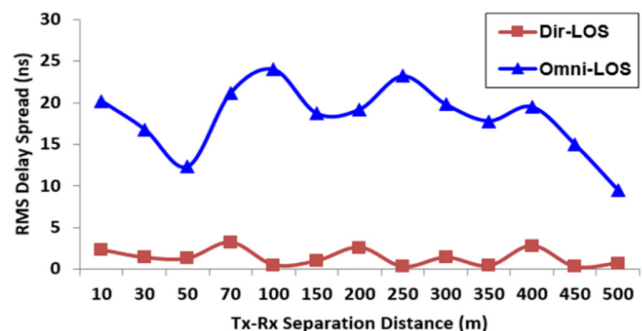


Fig. 4. Omnidirectional and directional RMS delay spread for a LoS urban microcell scenario.

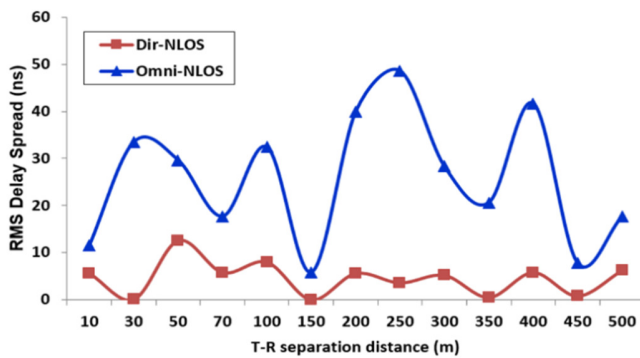


Fig. 5. Omnidirectional and directional RMS delay spread for a NLoS urban microcell scenario.

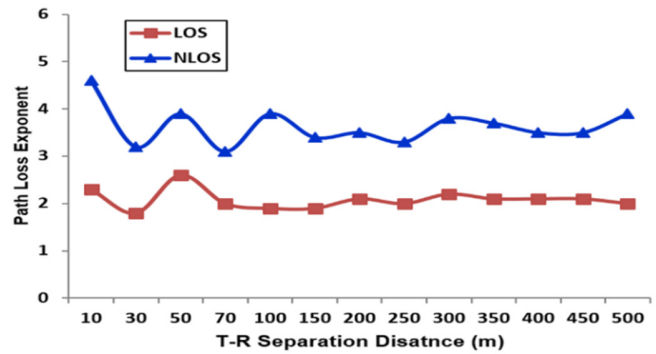


Fig. 7. PLE for MIMO system in omnidirectional LoS and NLoS urban microcell scenario.

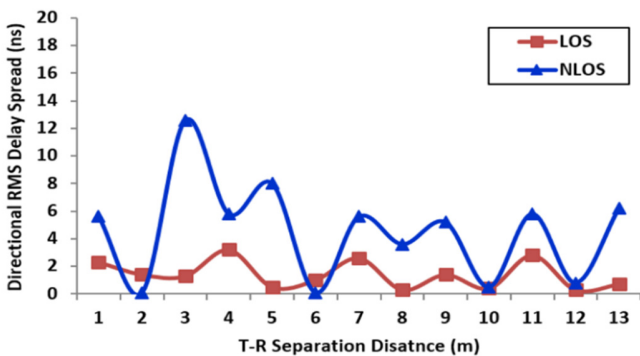


Fig. 6. Directional RMS delay spread for MIMO system in LoS and NLoS urban microcell scenario.

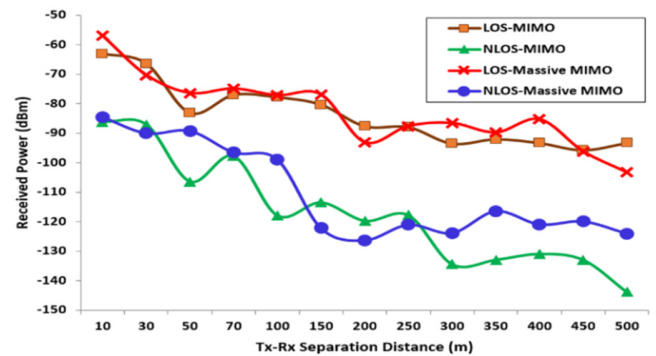


Fig. 8. Received power for MIMO and massive MIMO systems in omnidirectional LoS and NLoS urban microcell scenario.

The PLE confidentially describes the environment where the Tx and Rx are situated. It is an important parameter to indicate the propagation environment nature. In Figure 7, at 73GHz, the PLE for the MIMO system in omnidirectional LoS and NLoS urban microcell scenario is shown. Its values in LoS environment range between 2.6 and 1.8 which manifests a stronger power profile, while in NLoS environment, its values are between 3.1 and 4.6, leading to a weaker power profile. Additionally, Figure 7 shows that the PLE is more stable for LoS, especially for longer distances between the Tx and Rx, whereas less stability is shown for the NLoS case even for higher communication distances. The received power for MIMO and massive MIMO systems is illustrated in Figure 8. This Figure indicates that the received power is inversely proportional to the distance between Tx and Rx. As the distance increases, the path attenuation loss also increases which causes the signal power to diminish. On the other hand, for smaller separation distances between Tx and Rx, both MIMO and massive MIMO behave in an approximately similar way for LoS and NLoS. However, for longer distances, the massive MIMO system outperforms the MIMO system because the power in the massive MIMO has a very narrower beam than in the MIMO system, which means more active antenna means, more focused energy, and thus less attenuation. Figure 8 also shows that the average improvement of the received power in massive MIMO compared to MIMO is roughly 14% for long distances between 300 and 500m. Furthermore, massive MIMO system in LoS provides better performance than NLoS.

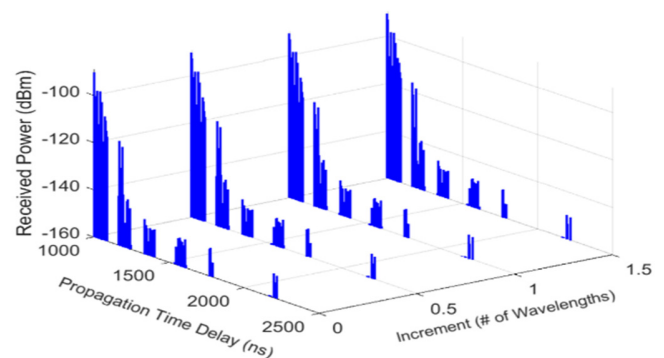


Fig. 9. Small scale PDPs at 73GHz in UMi LoS with 300m terrestrial separation and 4x4 MIMO system.

Figures 9-12 show the small scale Power Delay Profile (PDP) of the omnidirectional antenna using MIMO-LoS, MIMO-NLoS, massive MIMO-LoS, and massive MIMO-NLoS systems respectively. In Figures 9 and 10, it can be seen that there are 4 groups of omnidirectional components received at the Rx antenna and separated according to a specific value of the wavelength λ . The antenna spacing of Tx or Rx is adjusted to be 0.5λ even in the case of massive MIMO. The 4 groups are caused by the fact that the Rx uses 4 antenna elements for a 4x4 system. From Figures 9 and 10 it is also observed that the received power (dBm) decreases as propagation time delay RMS increases and that there is a noticeable gap between different multipath components as RMS delay spread increases. Also, due to the fact that the Rx uses 64 antenna elements for

the 64×64 system, as illustrated in Figures 11 and 12, it can be realized that there are 64 component groups at the Rx antenna.

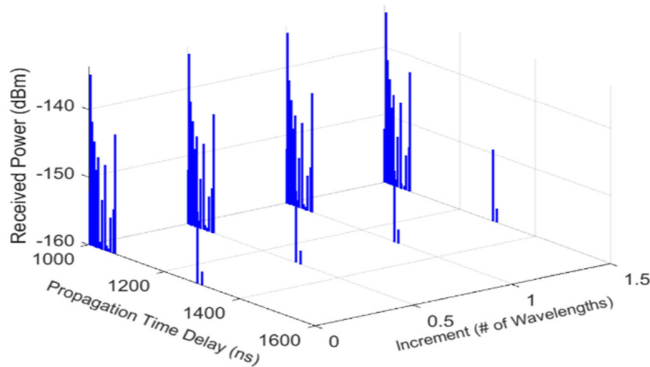


Fig. 10. Small scale PDPs at 73GHz in UMi NLoS with 300m terrestrial separation and 4×4 MIMO system.

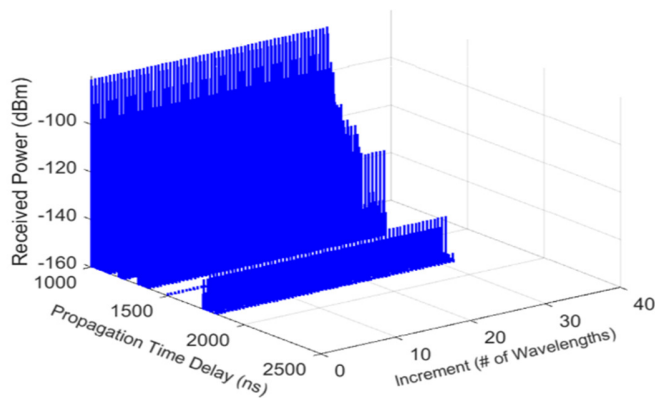


Fig. 11. Small scale PDPs at 73GHz in UMi LoS with 300m terrestrial separation and 64×64 Massive MIMO system.

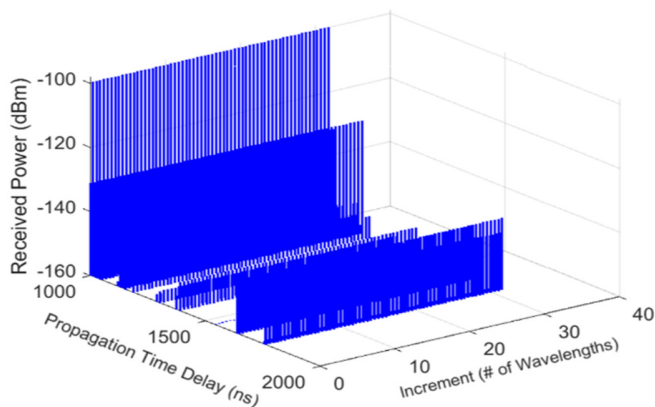


Fig. 12. Small scale PDPs at 73GHz in UMi NLoS with 300m terrestrial separation and 64×64 Massive MIMO system.

As a comparison, it is worth noticing that the strongest signal power for the 4 systems can be arranged in descending order as follows: (i) massive MIMO-LoS (Figure 11), (ii) MIMO-LoS (Figure 9), (iii) massive MIMO-NLoS (Figure 12), and (iv) MIMO-NLoS (Figure 10). Moreover, in the case of NLoS for both MIMO and massive MIMO, it is noticed that

less number of components in each group will be received at the Rx as shown in Figures 10 and 12, due to the fact that in the NLoS environment there are many blockage materials that act as signal attenuators and add losses to the signal power which in turn reaches the Rx with very low power, such that it can not be detected. In Figures 9 and 11, there are a lot of components in the case of LoS environment because no blockage material disturbs the signal power when it travels from the Tx to Rx. This environment does not impact highly the signal power, thus many components arrive to the Rx with higher magnitude than the one in the case of NLoS situation.

VII. CONCLUSION

This paper applied the MIMO and massive MIMO techniques to analyze the 5G propagation channel at 73GHz in an urban microcell scenario. The two systems, 4×4 MIMO and 64×64 Massive MIMO, have been assumed to examine the channel characteristics within two environment types, LoS and NLoS. Extensive simulations have been carried out through the Monte Carlo approach-based NYUSIM tool. The findings showed that the received power in the case of massive MIMO-LoS has higher magnitude than the other cases. The results also showed that for longer distances the massive MIMO outperforms the MIMO system due to the fact that using massive MIMO leads to more active antenna, which means more focused energy and thus less attenuation on the signal. In addition, it is revealed that the RMS delay spread and the PLE in LoS environment are more stable and suffer less fluctuation compared to the NLoS environment. In terms of the received power, the average percentage improvement in massive MIMO compared to MIMO is roughly 14% for long distances up to 500m.

REFERENCES

- [1] Z. A. Shamsan, "A Statistical Channel Propagation Analysis for 5G mmWave at 73 GHz in Urban Microcell," in *5th International Conference of Reliable Information and Communication Technology*, Langkawi, Malaysia, Dec. 2021, pp. 748–756.
- [2] F. Boccardi, R. W. Heath, A. Lozano, T. L. Marzetta, and P. Popovski, "Five disruptive technology directions for 5G," *IEEE Communications Magazine*, vol. 52, no. 2, pp. 74–80, Feb. 2014, <https://doi.org/10.1109/MCOM.2014.6736746>.
- [3] Z. A. Shamsan, "Dust Storm and Diffraction Modelling for 5G Spectrum Wireless Fixed Links in Arid Regions," *IEEE Access*, vol. 7, pp. 162828–162840, 2019, <https://doi.org/10.1109/ACCESS.2019.2951855>.
- [4] T. S. Rappaport *et al.*, "Millimeter Wave Mobile Communications for 5G Cellular: It Will Work!," *IEEE Access*, vol. 1, pp. 335–349, 2013, <https://doi.org/10.1109/ACCESS.2013.2260813>.
- [5] A. Al-Shuwaili and T. M. Jamel, "5G Channel Characterization at Millimeter-Wave for Baghdad City: An NYUSIM-based Approach," in *18th International Multi-Conference on Systems, Signals Devices*, Monastir, Tunisia, Mar. 2021, pp. 468–473, <https://doi.org/10.1109/SSD52085.2021.9429348>.
- [6] R. B. Ertel, P. Cardieri, K. W. Sowerby, T. S. Rappaport, and J. H. Reed, "Overview of spatial channel models for antenna array communication systems," *IEEE Personal Communications*, vol. 5, no. 1, pp. 10–22, Feb. 1998, <https://doi.org/10.1109/98.656151>.
- [7] S. S. Sun, T. S. Rappaport, R. W. Heath, A. Nix, and S. Rangan, "Mimo for millimeter-wave wireless communications: beamforming, spatial multiplexing, or both?," *IEEE Communications Magazine*, vol. 52, no. 12, pp. 110–121, Dec. 2014, <https://doi.org/10.1109/MCOM.2014.6979962>.

- [8] "NYUSIM Download Version 3.0," *NYU WIRELESS*. <https://wireless.engineering.nyu.edu/nyusim/> (accessed Jul. 07, 2021).
- [9] S. Ju, O. Kanhere, Y. Xing, and T. S. Rappaport, "A Millimeter-Wave Channel Simulator NYUSIM with Spatial Consistency and Human Blockage," in *IEEE Global Communications Conference*, Waikoloa, HI, USA, Dec. 2019, pp. 1–6, <https://doi.org/10.1109/GLOBECOM38437.2019.9013273>.
- [10] S. H. A. Momo and M. M. Mowla, "Statistical Analysis of an Outdoor mmWave Channel Model at 73 GHz for 5G Networks," in *International Conference on Computer, Communication, Chemical, Materials and Electronic Engineering*, Rajshahi, Bangladesh, Jul. 2019, pp. 1–4, <https://doi.org/10.1109/IC4ME247184.2019.9036692>.
- [11] S. Ju, Y. Xing, O. Kanhere, and T. S. Rappaport, "Millimeter Wave and Sub-Terahertz Spatial Statistical Channel Model for an Indoor Office Building," *IEEE Journal on Selected Areas in Communications*, vol. 39, no. 6, pp. 1561–1575, Jun. 2021, <https://doi.org/10.1109/JSAC.2021.3071844>.
- [12] H. Q. Ngo, *Massive MIMO: Fundamentals and System Designs*, vol. 1642. Linköping, Sweden: Linköping University Electronic Press, 2015.
- [13] P. Viswanath and D. N. C. Tse, "Sum capacity of the vector Gaussian broadcast channel and uplink–downlink duality," *IEEE Transactions on Information Theory*, vol. 49, no. 8, pp. 1912–1921, Aug. 2003, <https://doi.org/10.1109/TIT.2003.814483>.
- [14] D. Gesbert, M. Kountouris, R. W. Heath, C. Chae, and T. Salzer, "Shifting the MIMO Paradigm," *IEEE Signal Processing Magazine*, vol. 24, no. 5, pp. 36–46, Sep. 2007, <https://doi.org/10.1109/MSP.2007.904815>.
- [15] M. Kobayashi, N. Jindal, and G. Caire, "Training and Feedback Optimization for Multiuser MIMO Downlink," *IEEE Transactions on Communications*, vol. 59, no. 8, pp. 2228–2240, Aug. 2011, <https://doi.org/10.1109/TCOMM.2011.051711.090752>.
- [16] G. Caire and S. Shamai, "On the achievable throughput of a multiantenna Gaussian broadcast channel," *IEEE Transactions on Information Theory*, vol. 49, no. 7, pp. 1691–1706, Jun. 2003, <https://doi.org/10.1109/TIT.2003.813523>.
- [17] T. L. Marzetta, *Fundamentals of Massive MIMO*. Cambridge, UK: Cambridge University Press, 2016.
- [18] S. Sun, G. R. MacCartney, and T. S. Rappaport, "A novel millimeter-wave channel simulator and applications for 5G wireless communications," in *IEEE International Conference on Communications*, Paris, France, May 2017, pp. 1–7, <https://doi.org/10.1109/ICC.2017.7996792>.
- [19] S. Dahal, "Millimetre Wave for Fifth Generation of Wireless Communications," Ph.D. dissertation, Victoria University, Victoria, Australia, 2020.
- [20] S. H. A. Shah *et al.*, "Beamformed mmWave System Propagation at 60 GHz in an Office Environment," in *IEEE International Conference on Communications*, Dublin, Ireland, Jun. 2020, pp. 1–7, <https://doi.org/10.1109/ICC40277.2020.9149074>.
- [21] D. Pinchera, M. Migliore, and F. Schettino, "Compliance Boundaries of 5G Massive MIMO Radio Base Stations: A Statistical Approach," *IEEE Access*, vol. 8, pp. 182787–182800, 2020, <https://doi.org/10.1109/ACCESS.2020.3028471>.
- [22] R. Tang, X. Zhou, and C. Wang, "Kalman Filter Channel Estimation in 2×2 and 4×4 STBC MIMO-OFDM Systems," *IEEE Access*, vol. 8, pp. 189089–189105, 2020, <https://doi.org/10.1109/ACCESS.2020.3027377>.
- [23] F. O. Ombongi, H. O. Absaloms, and P. L. Kibet, "Energy Efficient Resource Allocation in Millimeter-Wave D2D Enabled 5G Cellular Networks," *Engineering, Technology & Applied Science Research*, vol. 10, no. 4, pp. 6152–6160, Aug. 2020, <https://doi.org/10.48084/etasr.3727>.
- [24] "5G; Study on channel model for frequencies from 0.5 to 100 GHz," ETSI, ETSI Technical Report 3GPP TR 38.901 version 14.0.0 Release 14, May 2017.
- [25] Z. A. Shamsan, "Rainfall and Diffraction Modeling for Millimeter-Wave Wireless Fixed Systems," *IEEE Access*, vol. 8, pp. 212961–212978, 2020, <https://doi.org/10.1109/ACCESS.2020.3040624>.
- [26] A. A. Alzamil, "Assessment of Uplink Massive MIMO in Scattering Environment," *Engineering, Technology & Applied Science Research*, vol. 10, no. 5, pp. 6290–6293, Oct. 2020, <https://doi.org/10.48084/etasr.3743>.